Available online at www.sciencedirect.com

SciVerse ScienceDirect

Physics Procedia 39 (2012) 767 – 775

Physics Procedia

LANE 2012

Optical monitoring in elaboration of metal matrix composites by direct metal deposition

M. Doubenskaia[a], I. Smurov[a,*], S. Grigoriev[b], M. Pavlov[b], E. Tikhonova[b]

[a]*Université de Lyon, Ecole Nationale d'Ingénieurs de Saint-Etienne (ENISE), DIPI Laboratory, 58 rue Jean Parot, 42023, Saint -Etienne Cedex 2, France*

[b]*Moscow State Technological University "Stankin", Vadkovsky per. 1, 127994 Moscow, Russia*

Abstract

Development of composites with multi-functional properties is a challenging problem that could be solved by laser cladding. The objective of the present work is to demonstrate the advantages of optical monitoring in optimizing deposition of carbide-reinforced metal matrix composites. Multi-wavelength pyrometer and infrared camera are applied to analyse high temperature heat – and mass transfer in the cladding zone. The influence of laser power, laser cladding speed and powder feeding rate on the brightness temperature are studied. The thermal images of the molten pool obtained by infrared camera for different TiC contents in the powder blend are analysed as well as the beads geometry, microstructure and microhardness.

Keywords: laser cladding; metal matrix composite; optical monitoring; pyrometry; infrared camera

1. Motivation

Direct Metal Deposition (DMD) is an automated laser cladding process to deposit a protective coating on the surface of a metallic part or layer-by-layer manufacturing of parts in a single-step process [1-4]. The objective of the present work is to demonstrate the advantages of optical monitoring in optimizing deposition of carbide-reinforced metal matrix composites [5-7]. Current trends in DMD are to produce multifunctional protective coatings which combine several exploitation properties, for example, wear and corrosion resistance, high electrical conductivity and abrasion resistance, thermal resistance and low friction coefficient, etc.

* Corresponding author. Tel.: +33-477-4375-61 ; fax: +33-477-7434-97 .
E-mail address: igor.smurov@enise.fr .

1875-3892 doi:10.1016/j.phpro.2012.10.099

Metal Matrix Composite (MMC) denotes a class of composites with at least two constituent materials one of which is a metal [8]. MMCs are applied, for example, in automotive and aerospace industry owing to enhanced high temperature strength, fatigue resistance, wear resistance and lightweight design [9]. Performance characteristics of a MMC object are influenced by the properties of the particulate reinforcement phase such as chemical composition, shape and size, properties as ingredient material, volume fraction and spatial distribution in the matrix [10].

2. **Experimental**

The present study was performed applying Trumpf DMD 505 laser cladding installation: The beam diameter $d_{0.86}$ increases linearly from 3.6 to 5 mm as the laser power varies from 2 to 5 kW. Experiments were carried out with scanning speed S = 0.4, 0.7, 1.0 m/min, laser power P = 3, 4, 5 kW, powder feeding rate F = 14, 25, and 36 g/min. The coating was produced by overlapping successive laser beads with hatch distance p = 3 mm. Gas flow rates were kept constant: $G_{carrier}$ (Ar/He) = 18/2 l/min, $G_{shaping}$ (Ar) = 10 l/min and G_{nozzle} (Ar/He) = 15/1 l/min.

MMC was developed from commercially available powders: (a) steel 16NCD13 (14NiCrMo13-4) by Sandvick Osprey Ltd. with -106+45 µm particle size; (b) titanium carbide by Testbourne with -80+40 µm particle. The powders were premixed in different proportions: 90/10; 95/5; 97.5/2.5 vol% of steel and of titanium carbide, respectively. The powder mixtures were deposited on cast iron substrate S235.

The originally developed pyrometers [11] were applied in the present study as well as the infrared camera FLIR Phoenix RDAS™ fixed with cladding head.

The pyrometers and infrared camera were calibrated with the help of the black body MIKRON M390 (maximum temperature 3000°C).

3. Results and discussion

3.1. Parametric analysis of laser cladding using optical diagnostics

Longitudinal profiles of brightness temperature in the zone of laser cladding are shown in Figs.1-3. One may note their predictable variations depending on the input parameters and almost the same average level of brightness temperature in the zone of bead formation.

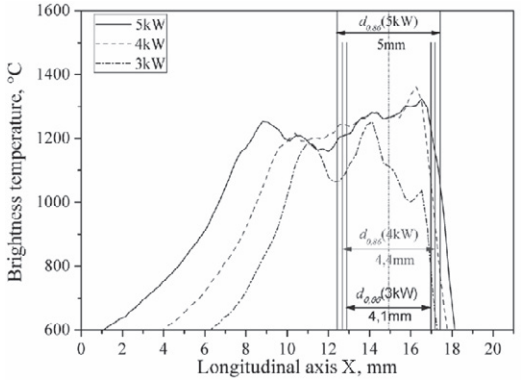

Fig. 1. Influence of laser power, *P*, on profiles of brightness temperature along the cladding bead. Cladding parameters: powder 16NCD13/TiC (90/10 vol%); *P* = var, *S* = 0.7 m/min, *F* = 15 g/min. Variation of beam diameter with laser power is indicated by $d_{0,86}$ parameter

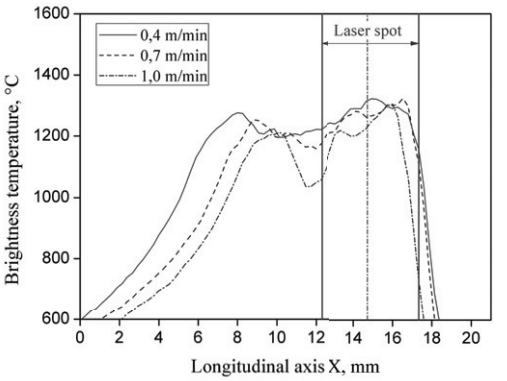

Fig. 2. Influence of scanning speed, *S*, on profiles of brightness temperature along the cladding bead. Cladding parameters: powder 16NCD13/TiC (90/10 vol%); *P* = 5 kW, *S* = var, *F* = 15 g/min

The monotonous increase of the sizes of heat affected zone (HAZ) with laser power is evident (Fig.1). The increase in the longitudinal direction is more pronounced than in the transversal one, that is related to elongated shape of the molten pool, which sizes are increasing with laser power, and the constant density of powder flux on its surface.

The monotonous temperature decrease with beam scanning speed (Fig.2) is similar to the one predicted by linear theory of heat transfer in case of Gaussian heat source moving on the surface of a semi-infinite body [3,4].

One may note the increase of molten pool size, which is defined by central temperature plateau, with powder feeding rate. It is interesting to note that the temperature of molten pool surface is not influenced by powder flow rate (Fig.3).

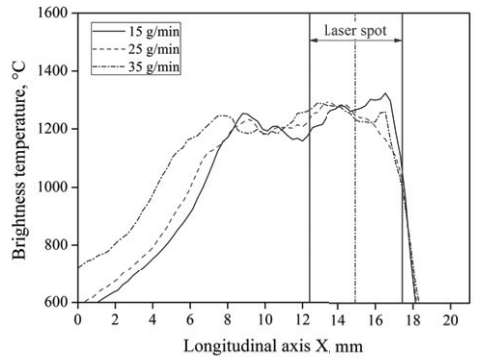

Fig. 3. Influence of powder feeding rate, *F*, on profiles of brightness temperature along the cladding bead. Cladding parameters: powder 16NCD13/TiC(90/10 vol%); *P* = 5 kW, *S* = 0.7 m/min, *F* = var

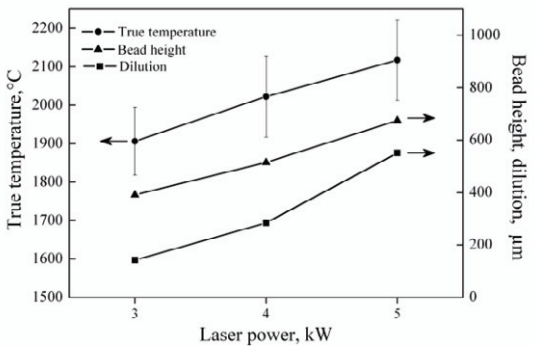

Fig. 4. Influence of laser power on true temperature and geometrical parameters of cladded bead obtained by multiwavelength pyrometer. Parameters: powder 16NCD13/TiC 90/10 vol%, *P* = var, *S* = 0.7 m/min, *F* = 15 g/min

In present experiments laser spot size is a function of laser power. That is why power density holds

practically at the same level. Also, the size of the laser spot in general defines the melt pool dimensions, i.e. the zone of powder integration into the cladding bead. The longitudinal size of molten pool can be defined from temperature profiles as the distance between local temperature maxima at the beginning of cladded bead (around 17 mm on X-axis) and the one before the monotone temperature decrease (in between 8 and 11 mm). These local temperature maxima correspond to the periphery areas of the molten pool, where oxides and ceramic powder are concentrated, and the neighbour solid phase areas that are oxidized. Both are characterised by higher emissivity values that the one of the molten pool.

The true temperature in the middle of cladding zone was restored using multiwavelength pyrometer and procedure is explained in [7]. The temperature was measured in the spot of 800μm situated near the laser beam center. Influence of laser power on true temperature and geometrical parameters of cladded bead are presented in Fig. 4. One may note quasi-linear increase of temperature, bead height and dilution with laser power. Using "calibration curves" similar to the ones presented in Fig.4, temperature monitoring can be used to control bead height and dilution.

It should be noted that the laser power, P, the scanning speed, S, and the powder feeding rate, F, have the similar effect on the bead height H. For the bead width, W, the major parameter is the laser power, P, that modifies spot size as well. The two-time rise of the laser power, P, from 2.5 up to 5 kW leads to the increase of the spot diameter $d_{0.86}$ from 3.8 to 5 mm and, thus, of the size of the melting pool. Under conditions applied in this study, variation of the powder feeding rate, F, does not lead to significant change of the diameter of the powder flow in the cladding area.

3.2. Brightness temperature at different TiC content

Looking at the complex temperature distributions registered by infrared camera, see Fig.5, one may note that it provides a lot of detailed information that is difficult to decode. Non-uniform temperature distribution could be related to the appearance of thin oxide films and their convective motion. Sharp temperature gradient at the head of molten pool (Figs. 5c, d) corresponds to the zone of particles injection into the molten pool. A particle at impact temperature depends on a number of factors including particle trajectory that defines its interaction with laser beam. Keeping in mind small size of a particle, it could be rapidly overheated to a temperature well superior than that of the molten pool. Under certain conditions, for certain trajectories of particles, their temperature at impact could well exceed the molten pool temperature. As infrared camera records the superposition of thermal emission from cladded bead and from particles-in-flight, this results in appearance of zones with elevated temperature.

The variation of brightness temperature with increasing content of ceramic component in the powder blend could be partly explained by the difference in their optical and thermal properties. Instability of injection of admixture when using premixed powder blends is a known problem as well. And, finally, there are visible differences in between consecutive images in the frames of the same series of experiments.

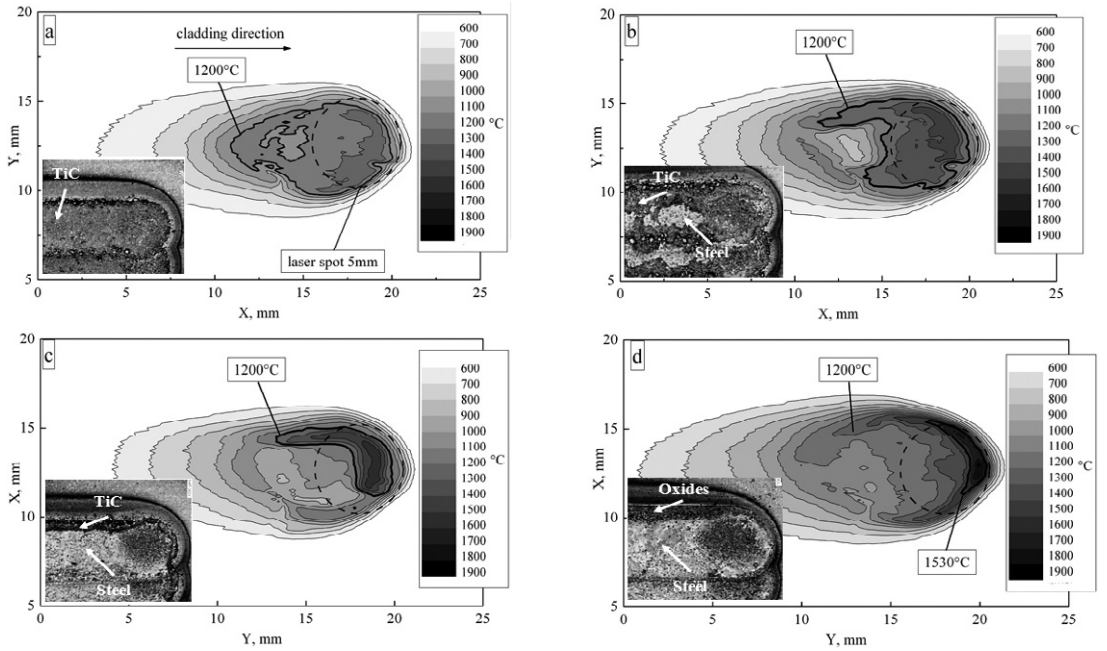

Fig. 5. Brightness temperature distribution for TiC contents in the powder 16NCD13/TiC (var vol%): (a) 90/10 (vol%); (b) 95/5 (vol%); (c) 97.5/2.5 (vol%); (d) 100/0 (vol%); Cladding parameters: $P = 5$ kW, $S = 0.7$ m/min, $F = 15$ g/min; powder 16NCD13/TiC (var vol%)

The following conclusions are retained after analysis of experimental results:

(a) There is the difference in the thickness of the cladded beads corresponding to different percentage of TiC in initial powder blend (Fig.6). It decreases from 0.85 mm for pure steel to 0.5 mm for 10% of TiC passing through 0.75 mm for 5% of TiC. The above values were found starting from about 20th mm of superposed beads when building height objects. On the other hand the bead height is almost the same for the first cladded layer.

(b) Practically the entire surface of the cladded bead is covered by TiC when its concentration in the powder blend reaches 10%. For 5% of TiC in powder mixture, it is found mainly in the periphery areas of cladded bead (Fig.5b).

(c) The temperature mapping of laser cladding zone by infrared camera reveals highest temperature gradients at the head of the bead without TiC injection while surface area with brightness temperature $T \geq 1200°C$ is relatively small. On the contrary, for 10% of TiC this zone is the largest one (Fig. 5a) but temperature gradients are lower.

It is not evident to explain the above regularities in a clear way, nevertheless certain hypothesis could be proposed: The presence of TiC layer on the surface of the previously cladded under-layer that represents a “substrate”, plays the role of a “thermal barrier” with lower thermal conductivity than for the pure steel. Also presence of TiC changes surface optical properties. During cladding the melt surface is partly covered by TiC powder (almost covered when 10% of TiC is injected) that remains in a solid state and can reject certain quantity of incoming powder. This results in decrease of size of the molten pool and the clad height. The trajectories of metallic and ceramic particles are not the same as well and their eventual collisions could modify distribution of particles density flux.

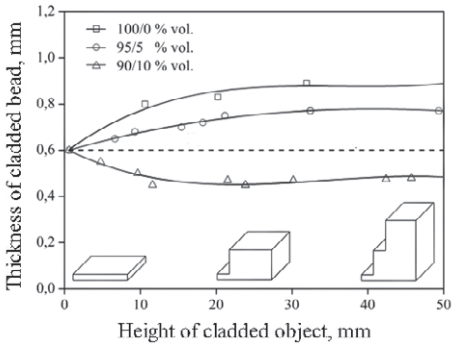

Fig. 6. Thickness of cladded bead versus height of cladded object. Thickness of the 1st cladded bead is 0.6 mm. Parameters: $P = 5$ kW, $S = 0.7$ m/min, $F = 14$ g/min, powder blend: 16NCD13/TiC (variable)

3.3. Metallographic analysis

Phase diagram of Fe-TiC system: 16NCD13 powder is a low-carbon low-alloy steel. To estimate at a first approximation the effect of titanium carbides, TiC, on the microstructure and the properties of the steel, an iron alloy with TiC could be considered [12].

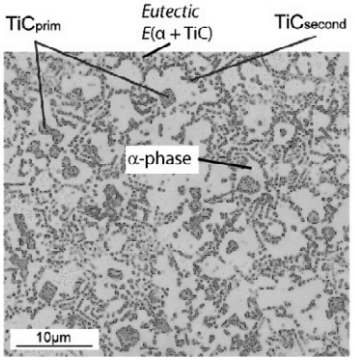

Fig.7. Microstructure of hypereutectic alloy from 16NCD13/TiC (90/10 vol%) powder mixture

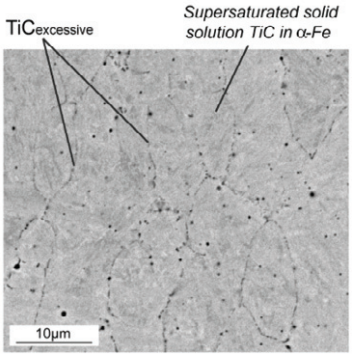

Fig. 8. Microstructure of hypoeutectic alloy from 16NCD13/TiC (97.5/2.5 vol%) powder mixture

The quasi-binary Fe-TiC section has a eutectic-type phase diagram with 3.8 wt% of TiC content in the eutectic. The maximum solubility of TiC in Fe is 0.6 wt%. Concentration of the elements dissolved in a solid solution increases with the cooling rate relatively to the equilibrium crystallization. These solid solutions are considered as metastable or supersaturated. During laser cladding, high cooling rates ($> 10^4$ K/s) contributes to the formation of a supersaturated solid solution of TiC in γ-phase [13].

To determine the influence of TiC on the microstructure and properties of the steel, the following contents of TiC in the steel were selected: 2.5 vol% (1.6 wt%) (hypoeutectic alloy); 5 vol% (3.2 wt%) (near-eutectic alloy), and 10 vol% (6.4 wt%) (hypereutectic alloy).

The hypereutectic alloy containing 10 vol% (6.4 wt%) of TiC consists of three structural components: 1 – primary titanium carbide TiC_{prim}; 2 – eutectic E (α + TiC); 3 – secondary titanium carbide TiC_{second} (Fig.7).

TiC_{prim} nucleated in the form of compact polyhedrons (small-scale dendrites) which become centers of the crystallization of the eutectic. The crystallization of the eutectic *E* (γ + TiC) is not equilibrium at high cooling rates that are typical for laser cladding. After the crystallization of TiC_{prim}, the liquid phase is depleted by titanium carbide near TiC_{prim} crystals. TiC in γ-phase has no time to completely diffuse because of a high cooling rate. As the result solid solution of TiC in γ-Fe is formed around TiC_{prim}. This process continues until the composition of the rest liquid phase reaches the eutectic ones, after that crystallization of the eutectic will start.

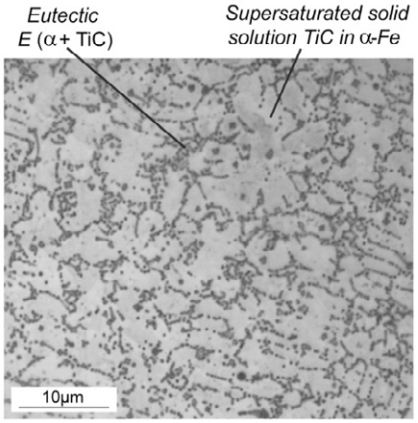

Fig. 9. Microstructure of near-eutectic alloy from 16NCD13/TiC (95/5 vol%) powder mixture

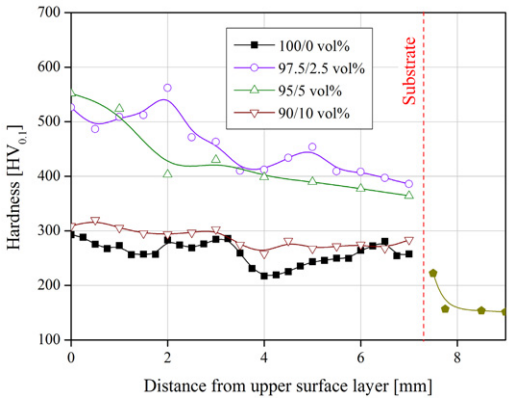

Fig. 10. Microhardness distribution of the MMC material versus distance from the upper surface layer and TiC volume fraction in the powder mixture

Secondary titanium carbides TiC_{second} precipitate in the eutectic phase due to a change in the solubility of TiC in the γ-phase from 0.6 up to 0.011 wt% in the solid state. However, these precipitations are difficult to identify even at a large variation of the solubility because their shape is very similar to the one of the eutectic.

The hypoeutectic alloy with 2.5 vol% (1.6 wt%) TiC content consists of two structural compounds: 1 – supersaturated solid solution TiC in α-Fe; 2 – excessive titanium carbides TiC (Fig.8).

The solubility limit of TiC in γ-Fe increases because of a high value of the supercooling, and the alloy turns to be γ-monophase. A supersaturated solid solution of TiC in γ-Fe forms. The excessive TiC precipitates at the grain boundaries because of the repeated heating of the metal by the upper cladded layers (Fig.8). The analysis of the distribution of the chemical elements showed a high concentration of titanium on the grain boundary in the region of the excessive TiC precipitation. The other elements in the alloy are distributed uniformly.

The structure of the near-eutectic alloy with 5 vol% (3.2 wt%) TiC content consists of two structural compounds: 1 – supersaturated solid solution TiC in α-Fe; 2 – eutectic *E* (α+ TiC) (Fig.9). The supersaturated solid solution of TiC in α-Fe forms in the similar way as in the alloy with 2.5 vol% TiC content. But the alloy is outside the α monophasic region because of higher TiC content. As a result, eutectic colonies in the lamellar and rod-like form precipitate at the dendrite boundaries (Fig.9). The precipitation of TiC_{second} does not occur due to the formation of supersaturated solid solution of TiC in γ-Fe. SEM analysis revealed a high concentration of titanium in the region of eutectic colonies. The other elements of the alloy are homogeneously distributed.

The microhardness tests of the MMC material yielded highly diversified results that indicates a considerable influence of micro structure on the properties of the samples (Fig. 10).

At the 2.5 and 5 vol% TiC content, the hypoeutectic alloy has a considerable microhardness that is higher by 40% in the middle and by 90% in the upper layers than that of the pure steel. The formation of the supersaturated solid solution of TiC in α-Fe with a strong distortion of the crystal lattice increases sharply the hardness. The microhardness of the hypoeutectic alloy close to the surface reaches up to $550HV_{0.1}$, but in the middle of cladded layer the microhardness decreases to $400HV_{0.1}$ because of the repeated heating of the alloy by the upper cladded beads. The precipitation of excessive TiC from the supersaturated solid solution of TiC in α-Fe reduces the distortion of the crystal lattice.

The microhardness of the hypereutectic alloy (10 vol% of TiC) insignificantly exceeds the one of the pure laser-cladded steel. The alloy structure consists from TiC_{prim} crystals surrounded by solid solution of TiC in α-Fe and eutectic *E* (α+ TiC). The microhardness of the α-phase depleted by titanium carbide is lower than that of the eutectic. As the volume fraction of the α-phase considerably exceeds the amount of the other phases, the alloy hardness is determined by a more plastic α-phase.

4. Conclusions

A carbide-reinforced MMC materials from a mixture of low-alloyed steel 16NCD13 and titanium carbide, TiC, powders was produced by laser cladding.

Multi-wavelength pyrometer and infrared camera were applied to analyse high temperature heat – and mass transfer in the cladding zone. The influence of laser power, laser cladding speed and powder feeding rate on the brightness temperature were studied. The thermal image of the molten pool obtained by infrared camera for different TiC contents in the powder blend was analysed as well as the beads geometry, microstructure and microhardness.

MMC with the low TiC content (2.5 and 5 vol%) have the highest microhardness (about 550 $HV_{0.1}$) due to the formation of the supersaturated solid solution TiC in α-Fe with a strong distortion of the crystal lattice. At the 10 vol% of TiC content, the material microhardness insignificantly exceeds that of the pure laser-cladded steel (about 280 $HV_{0.1}$) because of the nonequilibrium eutectic that is composed mainly of the ductile α-phase in the form of a rim around the TiC_{prim} crystals.

Acknowledgements

The study was supported by the grant of the Government of Russian Federation (decree N220).
D. Novicheknko helped in metallographic analysis.

References

[1] J. Mazumder, D. Dutta, N. Kikuchi, A. Ghosh: Closed loop direct metal deposition - art to part. In: Optics and Lasers in Engineering, 34 (2000), p. 397–414.

[2] E. Toyserkani, A. Khajepour, S. Corbin,: Laser cladding. CRS Press, Boca Raton, 2005.

[3] W. M. Steen, J. Mazunder: Laser material processing. London, 4th ed. (Springer-Verlag, London Limited, 2010).

[4] G. Gladush, I. Smurov: Physics of Laser Materials Processing: Theory and Experiment (Springer, 2011).

[5] G. Bi, A. Gasser, K. Wissenbach, A. Drenker, R. Poprawe: Identification and Qualification of Temperature Signal for Monitoring and Control in Laser Cladding. Opt. Lasers Eng., 2006, 44(12), p.1348-1359.

[6] J. Mazumder, D. Dutta, N. Kikuchi, A. Ghosh: Closed loop direct metal deposition: art to part. Opt. Lasers Eng., 2000, 34 (4-6), p.397-414.

[7] M. Doubenskaya, Ph. Bertrnd, I. Smurov: Optical Monitoring of Nd:YAG Laser Cladding. Thin Solid Films, 2003, 453-454C, p.447-485.

[8] J. Przybylowicz, J. Kusiński: Structure of laser cladded tungsten carbide composite coatings. In: Journal of Materials Processing Technology, 2001, 109, p. 154-160.

[9] K. Van Acker, D. Vanhoyweghen, R. Persoons: Influence of tungsten carbide particle size and distribution on the wear resistance of laser clad WC-Ni coatings. In: Wear, 2005, 258, p. 194-202.

[10] B.J. Kooi,Y. T. Pei, J. Th. M. De Hosson: The evolution of microstructure in a laser clad TiB-Ti composite coating. In: Acta Materialia, 2003, 51, p. 831-845.

[11] I. Smurov: Laser process optical sensing and control. IV International WLT-Conference on Lasers in Manufacturing 2007 (LIM-2007), Munich, Germany, 18-22 June 2007, p. 537- 546.

[12] Y. G. Gurevich, V.K. Narva, N. R.Frage: TiC-steel (Metallurgy, Moscow, 1988).

[13] J. C. Ion: Laser processing of engineering materials - principles, procedure and industrial application (Elsevier, Burlington, 2005).